Article

Spectroscopic and Electronic Structure Studies of Symmetrized Models for Reduced Members of the Dimethylsulfoxide Reductase Enzyme Family

Rebecca L. McNaughton, Booyong S. Lim, Sushilla Z. Knottenbelt, Richard. H. Holm, and Martin L. Kirk

J. Am. Chem. Soc., **2008**, 130 (14), 4628-4636 • DOI: 10.1021/ja074691b

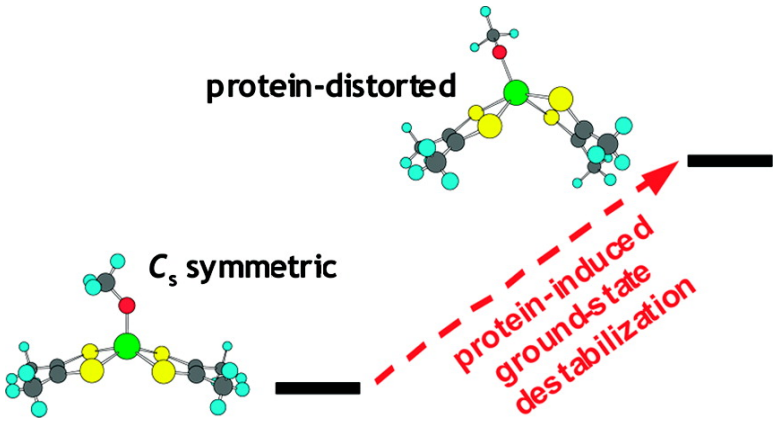

More About This Article

Additional resources and features associated with this article are available within the HTML version:

- Supporting Information
- Links to the 1 articles that cite this article, as of the time of this article download
- Access to high resolution figures
- Links to articles and content related to this article
- Copyright permission to reproduce figures and/or text from this article

View the Full Text HTML

J|A|C|S
ARTICLES
Published on Web 03/15/2008

Spectroscopic and Electronic Structure Studies of Symmetrized Models for Reduced Members of the Dimethylsulfoxide Reductase Enzyme Family

Rebecca L. McNaughton,[†,§] Booyong S. Lim,[‡] Sushilla Z. Knottenbelt,[†] Richard. H. Holm,*[,‡] and Martin L. Kirk*[,†]

Department of Chemistry, The University of New Mexico, MSC03 2060, 1 University of New Mexico, Albuquerque, New Mexico 87131, and Department of Chemistry and Chemical Biology, Harvard University, Cambridge, Massachusetts 02138

Received June 26, 2007; E-mail: holm@fas.harvard; mkirk@unm.edu

Abstract: Enzymes belonging to the dimethylsulfoxide reductase (DMSOR) family of pyranopterin Mo enzymes have a unique active-site geometry in the reduced form that lacks a terminal oxo ligand, unlike the reduced active sites of other pyranopterin Mo enzymes. Furthermore, the DMSOR family is characterized by the coordination of *two* pyranopterin-ene-1,2-dithiolate ligands in their active sites, which is distinctive among the other pyranopterin Mo enzymes but analogous to all of the currently known tungsten-containing enzymes. Electronic absorption, resonance Raman, and ground- and excited-state density functional calculations of symmetrized analogues of the reduced DMSOR active site ($[NEt_4][Mo^{IV}(QAd)(S_2C_2Me_2)_2]$ where Ad = 2-adamantyl; Q = O, S, Se) have allowed for a detailed description of Mo-bisdithiolene electronic structure in the absence of a strong-field oxo ligand. The electronic absorption spectra are dominated by dithiolene S → Mo charge-transfer transitions, and the totally symmetric Mo−S Raman stretch is observed at ∼400 cm^{-1} for all three complexes. These data indicate that the Mo-bisdithiolene bonding scheme in high-symmetry $[Mo(QAd)(S_2C_2Me_2)_2]^-$ complexes is not strongly perturbed by the apical QAd^- ligands, but instead, the dithiolene ligands define the t_{2g} ligand field splitting. The effects of conserved geometric distortions observed in DMSOR, relative to these high-symmetry models, were explored by spectroscopically calibrated bonding calculations, and the results are discussed within the context of electronic structure contributions to ground-state destabilization and transition-state stabilization. The specific electronic structure tuning of the endogenous amino acid ligation on the mechanism of DMSOR is also discussed.

Introduction

All forms of life utilize pyranopterin Mo enzymes to catalyze a variety of reactions involving both organic and inorganic substrates,[1,2] and these enzymes play key roles in the global metabolism of nitrogen- and carbon-containing molecules and the detoxification of sulfite, arsenite, and chlorate in many species.[2−5] The dimethylsulfoxide reductase (DMSOR) family[1,6,7] of enzymes are oxotransferases that catalyze an O atom transfer (OAT) from substrate to the reduced Mo active site, generating an oxidized mono-oxo Mo center (Scheme 1). The reduced active site is regenerated by two sequential coupled proton−electron transfer steps.[1] The presence of two pyranopterin ene-1,2-dithiolate ligands is a distinctive feature of the DMSOR enzyme family and is also characteristic of all currently known tungsten enzymes. Resonance Raman spectroscopy,[8−10]

Scheme 1

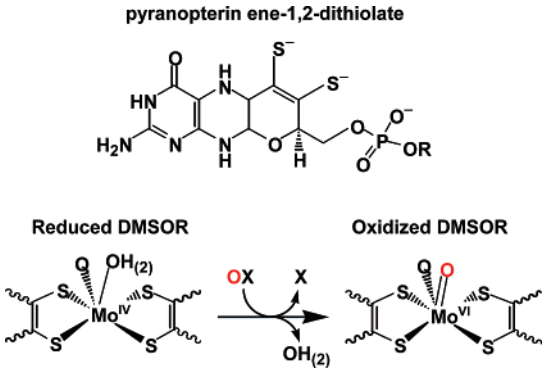

† The University of New Mexico.
‡ Harvard University.
§ Present address: Department of Chemistry, Northwestern University, Evanston, IL 60208.

(1) Hille, R. *Chem. Rev.* **1996**, *96*, 2757.
(2) Stiefel, E. I. *Molybdenum Enzymes, Cofactors, and Model Systems*; Stiefel, E. I., Coucouvanis, D., Newton, W. E., Eds.; American Chemical Society: 1993; pp 1−21.
(3) Kletzin, A.; Adams, M. W. W. *FEMS Microbiol. Rev.* **1996**, *18*, 5.
(4) Dobrovolsky, V. V. *Biogeochemistry of the World's Land;* Mir Publishers: 1994.
(5) Mackenzie, F. T.; Ver, L. M.; Sabine, C.; Lane, M.; Lerman, A. *Interactions of C, N, P and S Biogeochemical Cycles and Global Change*; Wollast, R., Mackenzie, F. T., Chou, L., Eds.; Springer-Verlag: 1993; pp 1−62.
(6) Kisker, C.; Schindelin, H.; Baas, D.; Retey, J.; Meckenstock, R. U.; Kroneck, P. M. H. *FEMS Microbiol. Rev.* **1998**, *22*, 503.
(7) Kisker, C.; Schindelin, H.; Rees, D. C. *Annu. Rev. Biochem.* **1997**, *66*, 233.
(8) Garton, S. D.; Temple, C. A.; Dhawan, I. K.; Barber, M. J.; Rajagopalan, K. V.; Johnson, M. K. *J. Biol. Chem.* **2000**, *275*, 6798.
(9) Garton, S. D.; Hilton, J.; Oku, H.; Crouse, B. R.; Rajagopalan, K. V.; Johnson, M. K. *J. Am. Chem. Soc.* **1997**, *119*, 12906.
(10) Bell, A. F.; He, X.; Ridge, J. P.; Hanson, G. R.; McEwan, A. G.; Tonge, P. J. *Biochemistry* **2001**, *40*, 440.

10.1021/ja074691b CCC: $40.75

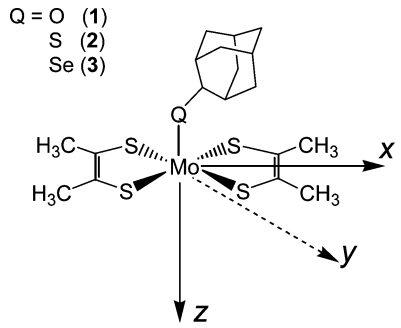

Figure 1. Structure of the model complexes in this study and the coordinate frame used in the analysis of the spectroscopy and DFT calculations. The *x*-axis bisects each dithiolene ligand, the *y*-axis is perpendicular to the plane of the page, and the *z*-axis is apical.

X-ray absorption spectroscopy,[11,12] isotopic labeling,[13] and a high resolution (1.3 Å) crystal structure[14] indicate a distorted trigonal prismatic mono-oxo $[Mo^{VI}O(O_{Ser})(S_2\text{-pyranopterin})_2]$ oxidized active site. X-ray and EXAFS studies of the reduced form of DMSOR are consistent with a desoxo $[Mo^{IV}(O_{Ser})(S_2\text{-pyranopterin})_2]$ active site geometry with water or hydroxide completing the first coordination sphere (Scheme 1).[11,12,15−17] Interestingly, the highly conserved serinate O donor found in DMSOR[1] is replaced by a cysteine S donor in nitrate reductase,[18] while in formate dehydrogenase a Se atom deriving from selenocysteine is bound to the Mo center.[19] It is anticipated, although no direct evidence has thus far been reported, that the nature of the protein-derived donor ligand in members of the DMSOR family modifies the energy of the Mo redox orbital and fine-tunes the effective nuclear charge of the metal center in order to poise the oxidation potential of the site at appropriate potentials for substrate-specific OAT catalysis and/or modulate the reduction potential for electron-transfer regeneration of the Mo^{IV} active site.

Structural and functional synthetic model complexes of the active sites unique to each pyranopterin Mo enzyme family have proven invaluable to the study of the intricate details of their enzymatic mechanisms.[20] Complexes of the general formula $[NEt_4][Mo^{IV}(QAd)(S_2C_2Me_2)_2]$ (Ad = 2-adamantyl; Q = O (**1**), S (**2**), or Se (**3**)) have been synthesized as symmetrized analogues of the reduced DMSOR active site,[21] allowing for a detailed investigation of Mo-bisditholene electronic structure in the absence of a strong-field oxo ligand (Figure 1). These complexes have a square pyramidal coordination geometry with effective C_{2v} symmetry for the first coordination sphere. Reactivity studies of these and related $[M^{IV}(QR)(S_2C_2R_2)_2]^{1-}$ complexes (M = Mo, W) show that this structural motif provides an analogue oxo-transfer reaction system with biologically relevant *N*-oxide and *S*-oxide substrates, yet they do not display reversible redox reactions, so values for the M^V/M^{IV} reduction potentials are inaccessible.[21−27] The oxo/sulfido-transfer studies indicate an associative transition state with reaction rates that are considerably slower than those found for the enzymes. The rate constants are highly dependent on substrate, although a uniform trend with substrate X−O bond dissociation energies was not observed.[28] Exploiting the greater stability of the isostructural tungsten analogues, reactivity studies on a series of $[W^{IV}(p\text{-OPh}-X')(S_2C_2(p\text{-Ph}-X)_2)]^{1-}$ complexes, where X and X′ were varied to affect the electron density at the metal center, were carried out in an effort to determine the rate-limiting step in the oxo-transfer mechanism of the model systems.[24] The results suggest that two transition states are present along the substrate reduction reaction pathway, implying a single intermediate. The first transition state is rate-limiting and involves the formation of a weak $W^{IV}\cdots OX$ interaction, which leads to an intermediate state in which the substrate is coordinated to the metal through the substrate O atom. The second transition state involves full W−O bond formation and O···X bond weakening coupled to the transfer of an electron pair to form the reduced product with a concomitant oxidation of the metal.

The energetics of the oxo-transfer half-reaction in model systems have been explored by three density functional theoretical studies which evaluated the binding of DMSO to geometry-optimized square-pyramidal $[Mo^{IV}(OCH_3)(\text{dithiolene})_2]^{1-}$ and the release of DMS (DMS = dimethylsulfide) after oxidation of the metal to form $[Mo^{VI}(O)(\text{dithiolene})_2]$.[29−31] Perhaps not surprisingly, given the five-coordinate reduced-enzyme model geometries used, the reaction profiles produced an associative mechanism with two transitions states, the second being rate-limiting, and a single intermediate. The structure of the intermediate formed via binding of the DMSO O to the metal center is best described as twisted trigonal prismatic. Webster et al. concluded that this distortion of the dithiolene ligands, which is similar to the distortion observed in DMSOR crystal structures, is an example of the entatic principle and primarily acts to destabilize the energy of the oxidized enzyme active site, which lowers the energy of the (second) transition state required for atom transfer and product formation.[29] The subsequent studies were in agreement with these conclusions. Thus, the rate-determining step in all three studies was calculated to be atom-transfer/product-release, not substrate binding, using *unconstrained* five-coordinate $[Mo(OCH_3)(\text{dithiolene})_2]^{1-}$ as the initial reduced active-site model.

(11) Temple, C. A.; George, G. N.; Hilton, J. C.; George, M. J.; Prince, R. C.; Barber, M. J.; Rajagopalan, K. V. *Biochemistry* **2000**, *39*, 4046.
(12) George, G. N.; Hilton, J.; Temple, C.; Prince, R. C.; Rajagopalan, K. V. *J. Am. Chem. Soc.* **1999**, *121*, 1256.
(13) Schultz, B. E.; Hille, R.; Holm, R. H. *J. Am. Chem. Soc.* **1995**, *117*, 827.
(14) Li, H. K.; Temple, C.; Rajagopalan, K. V.; Schindelin, H. *J. Am. Chem. Soc.* **2000**, *122*, 7673.
(15) George, G. N.; Colangelo, C. M.; Dong, J.; Scott, R. A.; Khangulov, S. V.; Gladyshev, V. N.; Stadtman, T. C. *J. Am. Chem. Soc.* **1998**, *120*, 1267.
(16) George, G. N.; Hilton, J.; Rajagopalan, K. V. *J. Am. Chem. Soc.* **1996**, *118*, 1113.
(17) Baugh, P. E.; Garner, C. D.; Charnock, J. M.; Collison, D.; Davies, E. S.; McAlpine, A. S.; Bailey, S.; Lane, I.; Hanson, G. R.; Mcewan, A. G. *J. Biol. Inorg. Chem.* **1997**, *2*, 634.
(18) Dias, J. M.; Than, M. E.; Humm, A.; Huber, R.; Bourenkov, G. P.; Bartunik, H. D.; Bursakov, S.; Calvete, J.; Caldeira, J.; Carneiro, C.; Moura, J. J. G.; Moura, I.; Romao, M. J. *Struct. Fold. Des.* **1999**, *7*, 65.
(19) Boyington, J. C.; Gladyshev, V. N.; Khangulov, S. V.; Stadtman, T. C.; Sun, P. D. *Science* **1997**, *275*, 1305.
(20) Enemark, J. H.; Cooney, J. J. A.; Wang, J.-J.; Holm, R. H. *Chem. Rev.* **2004**, *104*, 1175.
(21) Lim, B. S.; Holm, R. H. *J. Am. Chem. Soc.* **2001**, *123*, 1920.
(22) Goddard, C. A.; Holm, R. H. *Inorg. Chem.* **1999**, *38*, 5389.
(23) Sung, K. M.; Holm, R. H. *Inorg. Chem.* **2001**, *40*, 4518.
(24) Sung, K. M.; Holm, R. H. *J. Am. Chem. Soc.* **2002**, *124*, 4312.
(25) Wang, J.-J.; Kryatova, O. P.; Rybak-Akimova, E. V.; Holm, R. H. *Inorg. Chem.* **2004**, *43*, 8092.
(26) Jiang, J.; Holm, R. H. *Inorg. Chem.* **2005**, *44*, 1068.
(27) Wang, J.-J.; Tessier, C.; Holm, R. H. *Inorg. Chem.* **2006**, *45*, 2979.
(28) Sung, K. M.; Holm, R. H. *J. Am. Chem. Soc.* **2001**, *123*, 1931.
(29) Webster, C. E.; Hall, M. B. *J. Am. Chem. Soc.* **2001**, *123*, 5820.
(30) Thapper, A.; Deeth, R. J.; Nordlander, E. *Inorg. Chem.* **1999**, *38*, 1015.
(31) McNamara, J. P.; Hillier, I. H.; Bhachu, T. S.; Garner, C. D. *J. Chem. Soc., Dalton Trans.* **2005**, 3572.

Here we evaluate the electronic structure of the unique desoxo Mo-bisdithiolene active sites found in the DMSOR enzyme family, utilizing symmetrized model compound analogues of the reduced DMSOR active site probed by electronic absorption and resonance Raman spectroscopies and complemented by DFT bonding calculations. This work provides the first detailed bonding description of desoxo Mo-bisdithiolenes and evaluation of their redox chemistry through an understanding of metal−ligand covalency and valence ionization energy changes that occur as a function of the apical ligand donor. This establishes an electronic-structure basis for understanding oxo-transfer and electron-transfer reactivity in members of the DMSOR enzyme family.

Experimental Methods

General. The $[NEt_4][Mo^{IV}(QAd)(S_2C_2Me_2)_2]$ (Ad = 2-adamantyl; Q = O (**1**), S (**2**), or Se (**3**)) complexes were prepared as previously described.[21] All spectroscopic samples were prepared using dried and degassed solvents in a glovebag under a N_2 stream or in a glovebox in order to ensure sample integrity.

Electronic Absorption Spectroscopy. Electronic absorption spectra were collected on a Hitachi U-3501 UV−vis−NIR spectrophotometer capable of scanning a wavelength region between 185 and 3200 nm using a double-beam configuration at 2.0 nm resolution. The instrument wavelength was calibrated with reference to the 656.10 nm deuterium line. Background spectra were collected to correct for residual absorption due to the solvent or mulling agent and automatically subtracted from the sample spectrum by the Hitachi Grams software. Low temperature (11 K) spectra were collected using a Janis STVP-100 continuous flow cryostat mounted in a custom designed cradle assembly, and the sample temperature was monitored with a Lakeshore silicon-diode (PT-470) and regulated by a combination of helium flow and dual heater assemblies. Solid-state samples were prepared by grinding the complex into a fine powder, dispersing it into polydimethylsiloxane, and depositing a thin layer of the mixture between two 1.0 mm Infrasil quartz discs housed in a custom designed sample cell. Gaussian-resolution of spectral bands and corrections for light scattering were accomplished with the Grams 386 software package.

Resonance Raman Spectroscopy. Coherent Innova 70-5 Ar^+ ion (457.9−528.7 nm) and Coherent Innova 300C Kr^+ ion (406.7−676.4 nm) lasers were used as the excitation sources. The spectra were collected using laser excitation wavelengths of 406.7, 413.1, 457.9, 476.5, 488.0, and 514.5 nm. The scattered radiation was dispersed onto a liquid N_2 cooled 1″ Spex Spectrum One CCD detector using a Spex 1877E triple grating monochromator equipped with 600, 1200, and 1800 gr/mm holographic gratings at the spectrographic stage. The laser power at the sample was kept between 40 and 100 mW in an effort to prevent thermal degradation or photodegradation of the sample. Samples were prepared as finely ground powders and dispersed into finely ground $NaNO_3$ until the mixture was homogeneous. The prepared sample was then sealed in an NMR tube with a rubber septum and Parafilm. Room-temperature spectra were obtained with the sample tube placed in a modified NMR sample holder/spinner and collected using a 135° backscattering geometry.

Electronic Structure Calculations. All calculations were performed at the density functional level of theory using the Gaussian 98W software package.[32] These calculations employed the B3LYP hybrid functional with the 6-31G basis set on all nonmetal atoms with a polarization function added to the O, S, and Se atoms (6-31G*). The LANL2DZ basis set and LANL2 effective core potentials were used for Mo. DFT calculations of the $[Mo^{IV}(QAd)(S_2C_2Me_2)_2]^-$ complexes were performed using computational models with a methyl group in place of the adamantyl group. The coordinate frame used in the analysis of the output is shown in Figure 1 with the *z*-axis along the Mo−Q bond and the *x*-axis bisecting each dithiolene ligand. Single-point calculations with the crystallographically determined bond lengths and angles for the $MoQS_4C_4$ cores and geometry optimization calculations in C_s and C_1 symmetries were performed on all three of the computational models. Frequency calculations of the optimized structures were performed to ensure optimization to the minimum energy structures. The 40 lowest-energy excited states of the C_s-optimized $[Mo(QMe)(S_2C_2Me_2)_2]^-$ computational models were investigated by the time-dependent DFT method, as implemented by the Gaussian 98W program, which uses a single-excitation configuration interaction approach. This method has been found to give good qualitative results for transitions to low-lying states in closed-shell systems.[33,34] The calculations modeling the DMSOR reduced active site, using the computational model $[Mo^{IV}(OMe)(S_2C_2Me_2)_2]^-$, were all started from the crystallographic coordinates of the highest resolution crystal structure,[14] and various geometric constraints were imposed to explore the effects of the protein environment as detailed in the text.

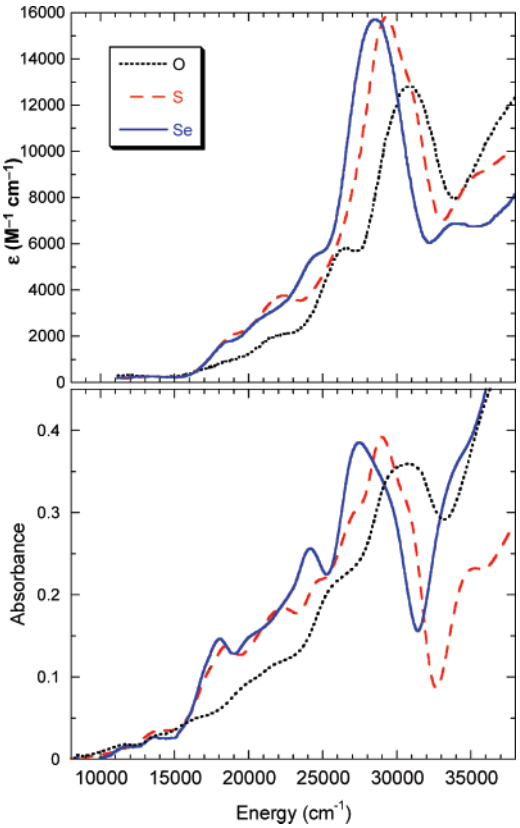

Figure 2. Electronic absorption spectra of **1**−**3** at room temperature as acetonitrile solutions (top) and at 11 K as solid-state mull (bottom).

Results and Analysis

Electronic Absorption Spectroscopy. Room-temperature CH_3CN solution and 11 K solid-state mull electronic absorption spectra of **1**, **2**, and **3** are shown in Figure 2. The solution spectra display the pattern of four maxima with increasing intensities toward higher energy that has been observed for many $[Mo^{IV}/W^{IV}(QR)(dithiolene)_2]^-$ complexes.[21,22,28,35−37] The bands above 15 000 cm^{-1} possess molar extinction coefficients greater than

(32) Gaussian 98, Revision A.7, Gaussian, Inc., Pittsburgh, PA, 1998.
(33) Casida, M. E.; Jamorski, C.; Casida, K. C.; Salahub, D. R. *J. Chem. Phys.* **1998**, *108*, 4439.
(34) Foresman, J. B.; Frisch, A. *Exploring Chemistry With Electronic Structure Methods;* Gaussian, Inc.: 1993.
(35) Lim, B. S.; Sung, K. M.; Holm, R. H. *J. Am. Chem. Soc.* **2000**, *122*, 7410.
(36) Sung, K. M.; Holm, R. H. *Inorg. Chem.* **2000**, *39*, 1275.
(37) Lim, B. S.; Donahue, J. P.; Holm, R. H. *Inorg. Chem.* **2000**, *39*, 263.

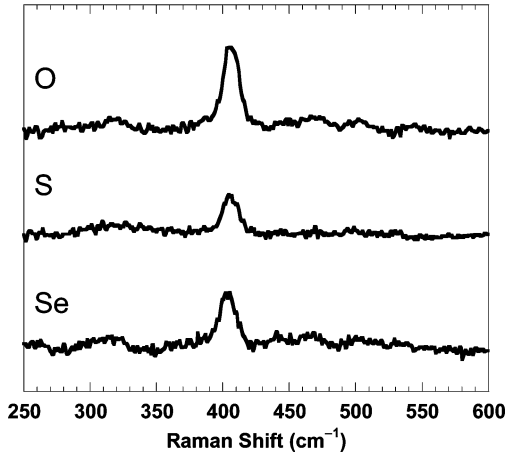

Figure 3. Solid-state resonance Raman spectra of $[NEt_4][Mo(QAd)(S_2C_2Me_2)_2]$ complexes in the 250−600 cm^{-1} region collected at room temperature using 514.5 nm excitation.

1000 M^{-1} cm^{-1}, indicating that they arise from charge-transfer transitions. The bands below ∼15 000 cm^{-1} have molar extinction coefficients estimated to be ∼200 M^{-1} cm^{-1}, indicative of ligand-field transitions. The solid-state spectra are generally similar to the solution spectra, indicating no major structural changes accompany solvation. The markedly narrower bandwidths observed as a result of the rigid and homogeneous molecular geometries in the solid state, coupled with vibrational narrowing at low temperature, allow for greater resolution of the individual transitions. There is evidence for 10 total bands in the spectrum of **2**, whereas **1** and **3** display 8 and 9 bands, respectively. A summary of the energies of the observed band maxima is presented in Table S1. Across the series, the observed maxima of bands above 15 000 cm^{-1} shift in energy as a function of the QAd^- donor according to O > S > Se. In contrast, the maxima of the bands below 15 000 cm^{-1} remain constant at ∼11 500 and ∼13 500 cm^{-1} for all three complexes. A similar trend is also observed in the solution spectra. These band shifts of 500−1000 cm^{-1} are quite small when compared to the >5000 cm^{-1} differences observed for O → Mo and S → Mo LMCT transitions in $(L-N_x)Mo^{V}O(OR/SR)$ complexes.[38,39]

Resonance Raman Spectroscopy. A single vibrational mode at ∼404 cm^{-1} was clearly observed in the resonance Raman spectra for all three complexes using excitation wavelengths of 406.7, 413.1, 457.9, 476.5, 488.0, and 514.5 nm. The spectra collected using 514.5 nm (19436 cm^{-1}) excitation are shown in Figure 3. The frequency of this band is in the range anticipated for the totally symmetric Mo−S_4 stretch.[40] In comparison, three bands are observed in the resonance Raman spectrum of $[MoO(S_2C_6H_4)_2]^{1-}$, with the totally symmetric stretch assigned at 358 cm^{-1}.[41,42] The totally symmetric Mo−S stretch for mono-oxo Mo^{IV}-bisdithiolene complexes has been assigned at 344 cm^{-1} for $[PPh_4]_2[MoO(S_2C_2(CN)_2)_2]$, 393 cm^{-1} for $[NEt_4]_2[MoO(S_2C_2(CO_2Me)_2)_2]$, and 356 cm^{-1} for $[PPh_4]_2$-$[MoO(S_2C_2H_2)_2]$.[43,44] No evidence for apical Mo−O, Mo−S, or Mo−Se modes were observed within the expected range for the singly bonded Mo−Q vibration, implying these modes are not coupled to electronic excitations in the ∼19 400−24 600 cm^{-1} region of the absorption spectra. Indications for additional weak bands are present at ∼315 cm^{-1}, ∼465 cm^{-1}, and between 1450 and 1550 cm^{-1} (the region in which the C−C stretch of the dithiolene C=C backbone is expected), but reliable data could not be collected due to complications from laser-induced sample decomposition.

Ground State Calculations. Electronic structure calculations of $[Mo^{IV}(QMe)(S_2C_2Me_2)_2]^-$ were performed for Q = O, S, and Se. These models possess effective C_{2v} core symmetry which will be used to describe the character of the resulting molecular orbitals.[45] Figure 4 displays the geometries of the computational models and the frontier molecular orbital energies resulting from single point calculations using the crystallographically determined bond lengths and angles for the $MoQS_4C_4$ cores. Optimized geometries were also calculated and compared to the crystal structures,[21] and the resulting bond lengths and angles are summarized in Table S2.

Each optimized structure resulted in a geometry with the methyl group of the apical ligand bisecting one of the dithiolene ligands as observed in the crystal structures of **1** and **3**.[46] The calculated bond lengths are consistently ∼2% longer than those determined by X-ray crystallography. With the exception of the Mo−Q−C angle, all the bond angles are within ∼1° of the crystal structure values. A decreased Mo-Q-C angle should more favorably orient one of the *p* orbitals on the Q donor to interact with the principal lobe of the Mo d_{z^2} orbital. Although this increases the overlap between these two orbitals, it does not have a marked effect on the orbital energies relative to the calculation at the crystal structure geometry. The atomic orbital character of the metal-based molecular orbitals is listed in Table 1 and electron density contour plots of the frontier molecular orbitals are shown in Figures S2−S4. The molecular orbital energies shift only slightly in the optimizations relative to those calculated using the crystal structure geometries, and neither the atomic orbital character of the Mo-based molecular orbitals nor the nature of the electron density in the frontier orbitals changes significantly. The overall bonding scheme is consistent with the diagram in Figure 4, except for the HOMO and HOMO-1 orbitals calculated for $[Mo(OMe)(S_2C_2Me_2)_2]^{1-}$. In this case, the orbitals exchange relative positions such that the HOMO is the $S_{op}(b_1)$ orbital and HOMO-1 is the Mo d_{xy} orbital, and they are separated in energy by only ∼0.1 eV.

The atomic orbital character and relative energies of the molecular orbitals are very similar across the series with the exception of the energy of the apical Q σ and π orbitals (Figure 4, dashed lines), an expected result due to differences in the valence ionization energies of O, S, and Se. The 8 dithiolene

(38) Carducci, M. D.; Brown, C.; Solomon, E. I.; Enemark, J. H. *J. Am. Chem. Soc.* **1994**, *116*, 11856.
(39) Rubie, N. D.; Kirk, M. L., unpublished results.
(40) Kirk, M. L.; McNaughton, R. L.; Helton, M. E. *Prog. Inorg. Chem.* **2003**, *52*, 111.
(41) McNaughton, R. L.; Helton, M. E.; Rubie, N. D.; Kirk, M. L. *Inorg. Chem.* **2000**, *39*, 4386.
(42) McNaughton, R. L. Electronic Structure Studies of Molybdenum-thiolate Complexes Related to Pyranopterin Molybdenum Enzymes. Ph.D. Dissertation, The University of New Mexico, Albuquerque, NM, 2002.
(43) Oku, H.; Ueyama, N.; Nakamura, A. *Inorg. Chem.* **1995**, *34*, 3667.
(44) Subramanian, P.; Burgmayer, S.; Richards, S.; Szalai, V.; Spiro, T. G. *Inorg. Chem.* **1990**, *29*, 3849.
(45) In keeping with literature precedence for pyranopterin molybdenum enzyme active sites and models, we chose to label the lowest energy Mo orbital as d_{xy} and the most destabilized Mo orbital as $d_{x^2-y^2}$. Thus, in C_{2v} symmetry the d_{xy} orbital transforms as a_1 and the $d_{x^2-y^2}$ orbital transforms as a_2.
(46) The position of the apical ligand methyl group, varied from bisecting a single dithiolene ligand (in the *xz* plane) to bisecting the two dithiolene ligands (in the *yz* plane), does not affect the general bonding scheme and only causes slight shifts of the molecular orbital energies, likely as a result of differential mixing of dithiolene S and apical chalcogen orbitals.

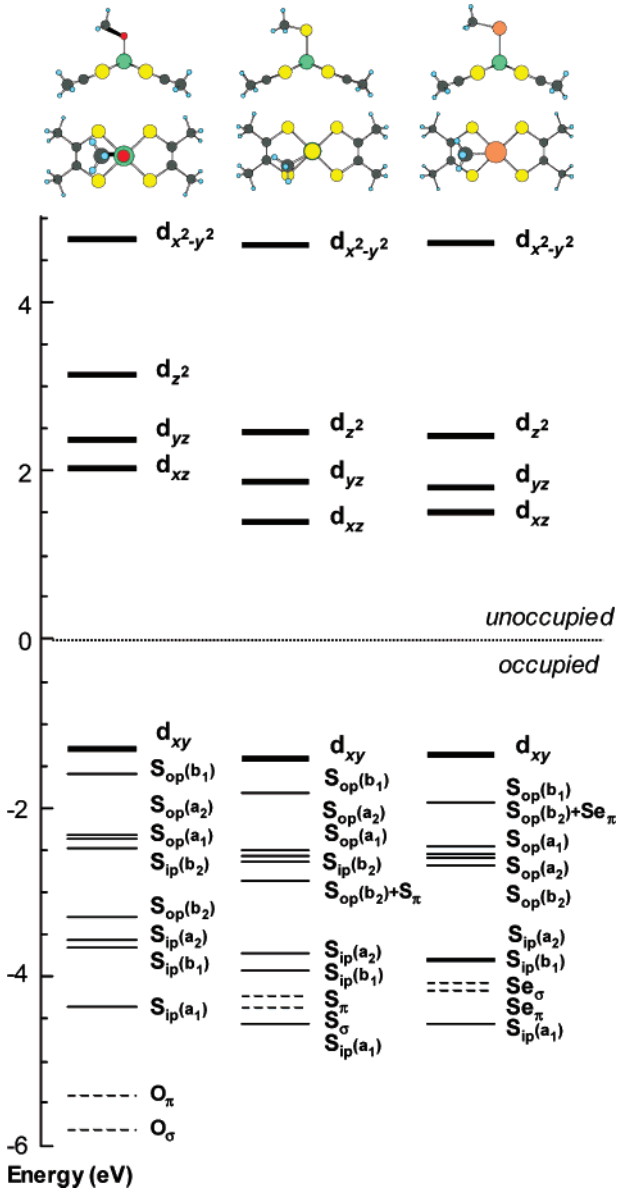

Figure 4. Molecular orbital energy diagrams resulting from DFT calculations of $[Mo(OMe)(S_2C_2Me_2)_2]^{1-}$ (left), $[Mo(SMe)(S_2C_2Me_2)_2]^{1-}$ (center), and $[Mo(SeMe)(S_2C_2Me_2)_2]^{1-}$ (right) in their crystal structure geometries (where Ad is replaced by Me). The Mo orbitals are presented as bold lines, and the ligand orbitals are presented as thin lines for the dithiolene-based orbitals or dashed lines for the apical Q^- orbitals.

S p orbitals available for bonding to Mo form eight symmetry adapted linear combinations (SALCs); four oriented in the dithiolene ligand plane, denoted S_{ip}, and four oriented perpendicular to the dithiolene plane, denoted S_{op} (see Figure S1). The relative energies of these S_{ip} and S_{op} orbitals are similar to those resulting from calculations of mono-oxo Mo−bisdithiolene complexes.[40,41] The Mo *d* orbital manifold (Figure 4, bold lines) is split such that the doubly occupied d_{xy} molecular orbital is lowest in energy[45] and isolated from the other Mo orbitals by approximately 1.5 eV, which is remarkably similar to the bonding scheme determined for mono-oxo Mo-bisdithiolene and Mo-tetrathiolate complexes.[41,42,47]

The Mo d_{xz} and d_{yz} orbitals remain nearly degenerate despite the fact that only a single π interaction is present between the apical Q p orbital and the d_{xz} orbital, which mixes ∼10% Q character into the d_{xz} orbital. The reduced π donation from the apical QMe^- donor to the d_{yz} orbital, relative to $[MoO(dithiolene)_2]^-$ complexes, is compensated for by increased donation from the dithiolene S donors. The σ donation of the apical chalcogen and the $S_{op}(a_1)$ SALC destabilize the d_{z^2} orbital. The contribution of each is approximately equal in the individual calculations, but the covalency is greater for the Q = S and Se calculations, which mixes two times more ligand character into the d_{z^2} molecular orbital, compared to the d_{z^2} orbital for Q = O. The $d_{x^2-y^2}$ orbital is the most destabilized Mo orbital as a result of the strong σ donation from the dithiolene ligands,[45] which mix ∼40% dithiolene S atomic orbital character into this molecular orbital.

Vibrational mode frequencies were calculated for each model in order to compare to the resonance Raman spectra of the model complexes. The calculated frequency of the totally symmetric Mo−S stretch, experimentally observed at ∼404 cm^{-1} for all three of the complexes, is nearly invariant in the frequency calculations as well, occurring at 396 cm^{-1} for **1** and 398 cm^{-1} for both **2** and **3**. All of the other calculated Mo−S stretching frequencies occur in the 300−400 cm^{-1} region where other Mo−S modes have been experimentally observed.[9,10,43,44] The average C=C stretching frequency calculated for all three

Table 1. Atomic Orbital Character (%) of Molecular Orbitals Resulting from DFT Optimization Calculations

molecular orbital[a]	Mo	S_4	Q	dithiolene[b]
	$Mo(OMe)(S_2C_2Me_2)_2]^{1-}$			
d_{xy}	69.0	14.4	0.4	30.6
d_{xz}	51.4	28.1	8.0	36.6
d_{yz}	49.3	34.0	5.0	40.3
d_{z^2}	56.7	19.6	13.7	25.3
$d_{x^2-y^2}$	25.5	43.7	0.0	74.4
	$Mo(SMe)(S_2C_2Me_2)_2]^{1-}$			
d_{xy}	67.1	14.3	1.7	31.3
d_{xz}	54.1	21.5	13.2	30.9
d_{yz}	43.5	38.4	3.1	46.4
d_{z^2}	47.7	19.0	26.7	23.7
$d_{x^2-y^2}$	20.9	37.5	0.1	79.0
	$Mo(SeMe)(S_2C_2Me_2)_2]^{1-}$			
d_{xy}	67.4	14.3	1.3	31.4
d_{xz}	54.1	22.2	13.2	31.6
d_{yz}	43.7	39.7	2.6	47.6
d_{z^2}	50.5	20.3	22.6	25.4
$d_{x^2-y^2}$	18.9	37.0	0.1	81.0
	$Mo(OMe)(S_2C_2Me_2)_2]^{1-}$ enzyme full opt			
d_{xy}	69.9	13.8	0.0	30.0
d_{yz}	54.1	28.2	4.7	36.2
d_{xz}	49.1	34.8	6.7	41.3
d_{z^2}	58.1	18.0	13.8	24.0
$d_{x^2-y^2}$	26.8	43.1	0.0	73.0
	$Mo(OMe)(S_2C_2Me_2)_2]^{1-}$ enzyme OPT 1			
d_{xy}	66.5	18.2	0.2	33.3
d_{yz}	55.3	28.7	5.9	35.7
d_{xz}	46.7	31.6	6.7	41.3
d_{z^2}	55.8	23.1	10.3	31.0
$d_{x^2-y^2}$	38.9	28.6	1.7	53.3
	$Mo(OMe)(S_2C_2Me_2)_2]^{1-}$ enzyme OPT 2			
d_{xy}	40.5	34.0	2.8	55.3
d_{yz}	59.7	23.3	7.2	30.2
d_{xz}	46.1	35.4	5.7	43.1
d_{z^2}	51.7	24.5	8.8	36.3
$d_{x^2-y^2}$	45.3	32.5	1.2	50.5

[a] Orbitals are listed in order of increasing energy. [b] Total dithiolene $(S_2C_2Me_2)_2$ contribution.

(47) McNaughton, R. L.; Tipton, A. A.; Rubie, N. D.; Conry, R. R.; Kirk, M. L. *Inorg. Chem.* **2000**, *39*, 5697.

computational models is 1580 cm^{-1}.[48] This is on the high end of the range observed for other dithiolene complexes (1450−1575 cm^{-1})[40,44] but is very close to the larger of the two observed C═C stretching frequencies in the resonance Raman spectrum of reduced DMSOR (1572 cm^{-1}).[9] A complete account of the calculated frequencies and symmetries of these modes are reported in Figure S5.

Excited State Calculations. Excited states of the $[Mo(QMe)(S_2C_2Me_2)_2]^{1-}$ computational models were investigated using time-dependent DFT performed at the C_s optimized geometries, the highest symmetry possible for these calculations. The energies and relative oscillator strengths of the calculated excited states are depicted as red bars in Figure 5, and the excitation energies, oscillator strengths, state symmetries, and primary orbital character of the dominant one-electron transition contributing to each of the 11 lowest energy states (with oscillator strength greater than 0.0001) are given in Table S3. The results are qualitatively similar for all three calculations, such that the oscillator strength of the most intense transition is at least 2-fold greater than any of the others. The predicted energies of these transitions decrease as Se < S < O, matching the observed trend of the most intense band in the electronic absorption spectra of **1**−**3**. The two lowest energy transitions are predicted to possess very low oscillator strengths, in agreement with the two weak ($\epsilon \approx 200$ M^{-1} cm^{-1}) bands in the low-energy region of the electronic absorption spectra. Four transitions with calculated oscillator strengths greater than 0.01 lie between the two very weak transitions and the most intense transition, consistent with the observed absorption intensities which increase toward higher energy with a dominant maximum at ∼30 000 cm^{-1}. Inspection of the molecular orbital electron density contours resulting from the time-dependent DFT calculations indicate that the symmetries of the molecular orbitals approach an effective C_{2v} symmetry. This allows for an ascent in symmetry from the C_s symmetry used for the calculations to C_{2v} symmetry for the analysis. Thus, the transformation properties of the orbitals are $a' \rightarrow a_1$, b_1 and $a'' \rightarrow b_2$, a_2. It is important to note that none of these predicted transitions directly involves the apical ligand orbitals, and transitions originating from orbitals with primarily apical ligand character only contribute appreciably to excited states at energies greater than 35 000 cm^{-1}. Three ligand field transitions ($d_{xy} \rightarrow d_{xz}$, $d_{xy} \rightarrow d_{yz}$, and $d_{xy} \rightarrow d_{z^2}$) are predicted at low energy in each calculation. The other states derive from LMCT transitions which originate from dithiolene-based molecular orbitals to the lowest-energy unoccupied metal d_{xz}, d_{yz}, and d_{z^2} orbitals. One-electron promotions between the dithiolene-based orbitals and the three lowest lying unoccupied metal orbitals are the transitions with the greatest calculated oscillator strength. These calculations predict that a high density of states will contribute to the optical absorption spectra of the three complexes, as exemplified by the small ∼7000 cm^{-1} separation of the first five most intense transitions. Three of these five transitions with large calculated oscillator strengths are *x*-polarized transitions in C_{2v} symmetry. The *x*-axis bisects each dithiolene ligand in this coordinate frame such that the electron density distribution along this axis is more extended than along the *y*-axis. The extended π conjugation of the dithiolene ligands along the *x*-axis has been suggested to induce a larger change in the electric dipole moment for transitions polarized along this axis and therefore show greater absorption intensity.[40,49] In summary, all of the states with calculated oscillator strengths greater than 0.01 are electric-dipole allowed in C_{2v} symmetry and are associated with transitions from dithiolene-based SALCs to the out-of-plane Mo d_{xz}, d_{yz}, or d_{z^2} orbitals.

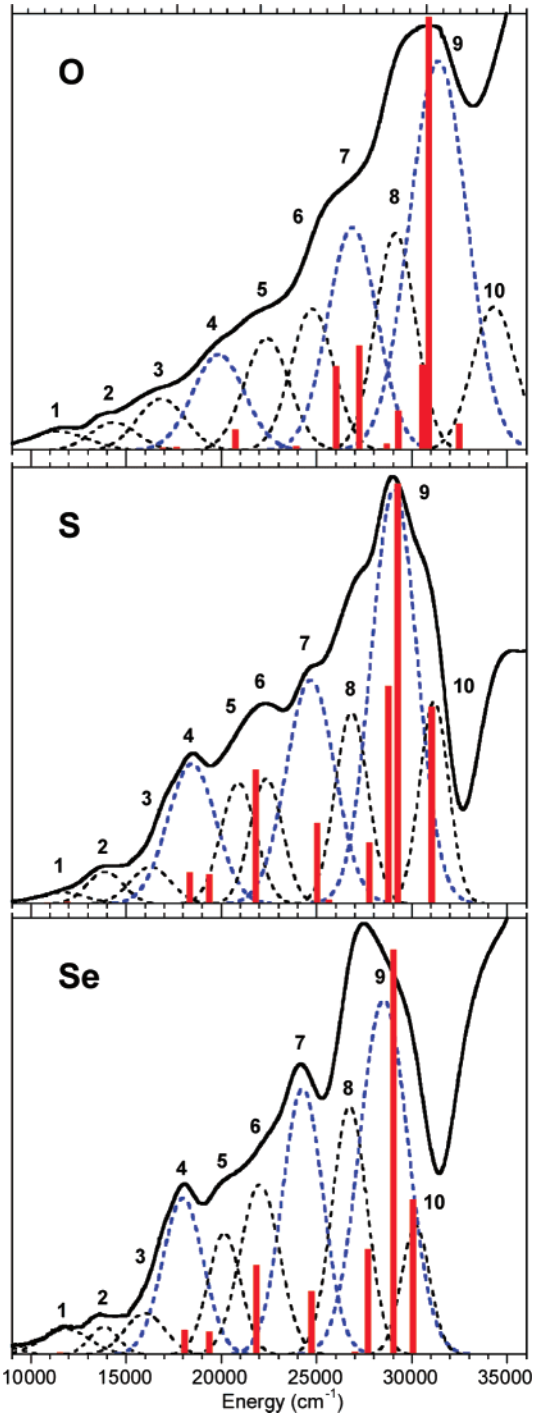

Figure 5. Gaussian-resolved solid-state electronic absorption spectra of **1**−**3**. The *x*-polarized transitions are shown in blue. The red bars indicate the energies and relative oscillator strength intensities of the excited states calculated by time-dependent DFT. Note that the TDDFT transition energies have not been shifted on the energy axis.

Gaussian Resolution and Band Assignments. It is logical to expect the same number of transitions for each complex in the 10 000−35 000 cm^{-1} region of the absorption spectra given

(48) Scaling factor of 0.9613 used per ref 34.

(49) Herman, Z. S.; Kirchner, R. F.; Loew, G. H.; Muellerwesterhoff, U. T.; Nazzal, A.; Zerner, M. C. *Inorg. Chem.* **1982**, *21*, 46.

Table 2. Band Energy Maxima and Assignments of the Gaussian-Resolved Electronic Absorption Spectra of $[Mo(QAd)(S_2C_2Me_2)_2]^-$ Complexes

band	O	S	Se	assignment
1	11 370	11 640	11 700	$d_{xy} \rightarrow d_{xz}$
2	14 340	13 880	13 810	$d_{xy} \rightarrow d_{yz}$
3[a]	16 830	16 270	16 250	$S_{op}(b_1) \rightarrow d_{xz}$
				$d_{xy} \rightarrow d_{z^2}$
4	19 860	18 440	18 020	$S_{op}(a_1) \rightarrow d_{xz}(b_1)$
5	22 370	20 870	20 080	$S_{ip}(b_2) \rightarrow d_{xz}(a_1)$
6	24 760	22 340	22 090	$S_{op}(a_2) \rightarrow d_{xz}(b_1)$
7	26 880	24 680	24 240	$S_{op}(b_1) \rightarrow d_{z^2}(a_1)$
8	29 120	26 810	27 040	$S_{ip}(b_2) \rightarrow d_{yz}(b_2)$
9	31 380	29 060	29 120	$S_{op}(a_2) \rightarrow d_{yz}(b_2)$
10	34 290	31 150	30 320	$S_{op}(a_1) \rightarrow d_{z^2}(a_1)$

[a] Two transitions are expected in this energy region, but only one maximum is clearly observed.

the similar spectral features observed across this series and for other $[Mo(QR)(dithiolene)_2]^{1-}$ complexes. At least 10 bands are apparent in the low temperature solid-state absorption spectrum of **2**; therefore 10 Gaussian bands were used to deconvolute each low-temperature spectrum, and these are displayed in Figure 5. The Gaussian resolution of the spectra is consistent across the series and clearly shows that the absorption intensity is primarily dominated by bands 4, 7, and 9. Reasonable assignments for these bands are detailed below based on the application of group theory in conjunction with the results of the ground-state and excited-state DFT calculations. The maxima of the individual Gaussian bands used to fit the spectra and their assigned electronic transition are shown in Table 2.

The relative energies of the absorption bands observed below ~35 000 cm^{-1} can be correlated with the inherent ionization energies of the O, S, and Se donor atoms of the apical QAd^- ligand despite the assignment of all of the charge-transfer transitions as $S_{dithiolene} \rightarrow Mo$ in nature. It is expected that Q → Mo LMCT transitions would shift as a function of Q more than the ~2000 cm^{-1} that is experimentally observed for these complexes. For example, oxomolybdenum complexes with diolate ligands substituted for dithiolate/dithiolene ligands possessed O → Mo LMCT transitions that were shifted ~5000 cm^{-1} to higher energy than the corresponding S → Mo transitions.[38] The assignment of the observed spectral features in **1**−**3** as $S_{dithiolene} \rightarrow Mo$ charge-transfer excitations is also supported by the resonance Raman spectra which show enhancement of the totally symmetric Mo−S stretch at every accessible excitation wavelength under the broad absorption envelope. That the lowest energy charge-transfer bands are $S_{dithiolene} \rightarrow Mo$ in nature is further supported by the ground-state DFT calculations that show the apical QAd-based molecular orbitals to be among the most stabilized of the bonding frontier molecular orbitals. The time-dependent DFT calculations also suggest that transitions involving the QAd-based molecular orbitals should occur at energies greater than 35 000 cm^{-1}. However, *mixing* of the O/S/Se orbitals with the dithiolene SALCs is the likely origin of the observed shifts in absorption energies. Orbital mixing between the apical QAd^- ligand and the dithiolenes is anticipated since the symmetries of the dithiolene SALCs ($a' = a_1, b_1$ and $a'' = a_2, b_2$ in C_{2v} symmetry) are the same as those for the σ and π orbitals of the apical QAd^- ligands in C_s symmetry (a' and a'').

The spectroscopic results, generalized bonding description, and results of DFT calculations allow for detailed band assignments to be made for $[Mo(QR)(S_2C_2Me_2)_2]^{1-}$ complexes (Table 2). Bands 1 and 2 are assigned as $d_{xy} \rightarrow d_{xz}$ and $d_{xy} \rightarrow d_{yz}$ ligand field transitions, respectively, and their weak absorption intensity and low energy support this assignment. Band 3 is most likely a combination of two transitions. The $d_{xy} \rightarrow d_{z^2}$ ligand field transition is expected in this region, but the observed enhanced intensity of the absorption indicates that some charge-transfer character may also be present. Therefore, we propose that a weak *z*-polarized $S_{op}(b_1) \rightarrow d_{xz}$ LMCT transition is the dominant contributor to the absorption intensity of band 3. The most intense charge-transfer bands are anticipated to be $S_{in-plane} \rightarrow Mo_{in-plane}$ or $S_{out-of-plane} \rightarrow Mo_{out-of-plane}$ and be *x*-polarized along the dithiolene−dithiolene axis.[40] Thus, the *x*-polarized $S_{op}(a_1) \rightarrow d_{xz}$, $S_{op}(b_1) \rightarrow d_{z^2}$, and $S_{op}(a_2) \rightarrow d_{yz}$ LMCT transitions are assigned as bands 4, 7, and 9, respectively, as these are the most intense transitions observed in the electronic absorption spectra. Tentative assignments for bands 5, 6, 8, and 10 have been made based on the relative dipole allowedness of these transition in C_{2v} symmetry, the orbital overlap predicted by the ground state DFT calculations, and the calculated oscillator strengths from the excited state DFT calculations (Table S3).

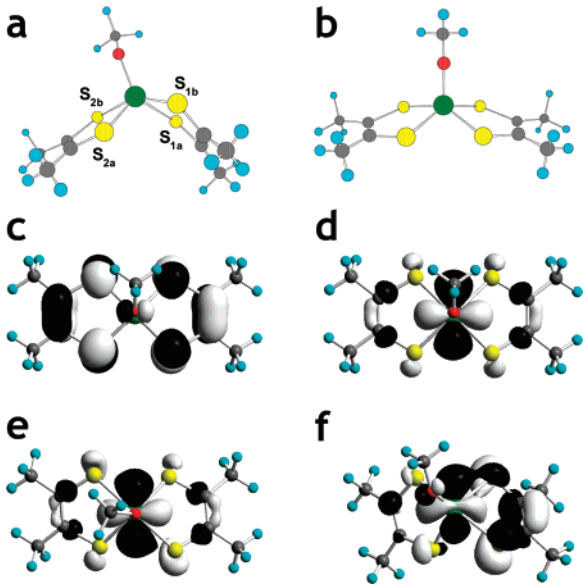

Figure 6. (a) DMSOR active-site crystal structure, (b) optimized active-site structure, (c) HOMO of optimized active-site structure, (d) HOMO-1 of optimized active-site structure, (e) HOMO of optimized active-site with dithiolene twist constrained, denoted OPT1, and (f) HOMO of optimized active-site with dithiolene twist and O distortion constrained, OPT2.

DFT Calculations of the Reduced DMSOR Active Site. Using the same computational method as above that has been rigorously calibrated by spectroscopy (vide supra), calculations were performed on a model of the reduced DMSOR active site, $[Mo^{IV}(OMe)(S_2C_2Me_2)_2]^{1-}$, starting from crystal structure bond lengths and angles (Figure 6a). Note that this computational model is missing the coordinated water or hydroxide that has been determined to complete the coordination sphere of reduced DMSOR. As such, it represents the geometry of the active site *after* dissociation of bound H_2O/OH^- and poised for attack by the substrate (i.e., assuming a dissociative mechanism). Initially, a full optimization was performed from the crystal structure geometry starting point to provide an energetic zero-point reference for the enzyme geometry. This optimization resulted in a symmetric geometry (Figure 6b) with the four dithiolene S

atoms coplanar, and the methoxy O apical with the methyl group bisecting the two dithiolene ligands, in contrast to the optimization starting from the model complex geometry where the methyl group bisects one dithiolene ligand. This has little effect on the composition of the metal-based molecular orbitals (Table 1). The HOMO (Figure 6c) has dominant out-of-plane dithiolene character and lies just 0.16 eV above the formal Mo d_{xy} orbital (Figure 6d), similar to the optimization of $[Mo(OMe)(S_2C_2Me_2)_2]^{1-}$ starting from the model complex crystal structure geometry.

This square-pyramidal C_{2v} symmetric species differs considerably from the highly distorted low-symmetry enzyme active site, and therefore, a series of calculations imposing constraints on specific angles were carried out to explore how the protein environment affects the active site geometry and electronic structure. First, denoted as OPT1, the $S_{1a}-S_{1b}-S_{2b}-S_{2a}$ dihedral angle of the dithiolene ligands was constrained to the angle observed in the protein crystal structure (142.5°) and the rest of the model was reoptimized. This resulted in only a minor energetic destabilization of 0.052 eV (1.2 kcal/mol) but a change in the energy order of the HOMO and HOMO-1 such that the HOMO is now the Mo-based d_{xy} (Figure 6e). The atomic orbital character of the metal-based molecular orbitals change little compared to those from the fully optimized calculation (Table 1) except for the $d_{x^2-y^2}$ orbital. The dithiolene twist decreases the dithiolene character in this orbital by ∼20%. Further inspection of this optimized structure revealed that the methoxy group again optimized to an apical position equivalent between the two dithiolene ligands, as opposed to canted toward a single dithiolene away from the symmetric apical position, as observed in the crystal structure of the enzyme (Figure 6a). Next, in addition to the dithiolene twist, the $O-Mo-S_{1a}-C$ dihedral angle was constrained to 146.2° to preserve the cant of the serine ligand observed in the crystal structure of the enzyme (denoted OPT 2). This resulted in a much larger destabilization, 0.99 eV (23 kcal/mol) compared to the fully optimized reference point, and a significant change of the atomic orbital character in the HOMO (Figure 6f). The d_{xy} orbital in this asymmetric model has ∼20% more dithiolene ligand character and a substantial increase in O atomic orbital character, 14 times more than the OPT1 geometry.[50]

Discussion

Desoxo Mo-Bisdithiolene Bonding. The square pyramidal geometries of the $MoQS_4$ cores found in $[Mo(QR)(S_2C_2Me_2)_2]^{1-}$ models are similar to the $MoOS_4$ cores of mono-oxo $[MoO(dithiolene)_2]^{0,1-,2-}$ complexes, and this is reflected in the ligand field splitting of their Mo *d*-orbital manifolds.[40−42] The dominant metal−ligand interactions in **1**−**3** are σ-type $d_{x^2-y^2}$-S^{σ} and d_{z^2}-Q^{σ} orbital interactions that destabilize the Mo $d_{x^2-y^2}$ and d_{z^2} orbitals relative to the d_{xz}, d_{yz}, and d_{xy} orbitals. Unlike mono-oxo $[MoO(dithiolene)_2]^{n-}$ complexes that have three *p* orbitals on the terminal oxo ligand available for bonding with Mo, only two *p* orbitals on the O, S, or Se of the QAd^- ligand are available for bonding because the third *p* orbital is involved in Q−C σ-bonding with the adamantyl carbon and is therefore unavailable for significant bonding interactions to Mo. The Mo−S σ-antibonding interactions destabilize the $d_{x^2-y^2}$ orbital more than the d_{z^2} orbital, which has only one σ interaction from the apical QAd^- ligand. The second *p* orbital of the apical QAd^- ligand is orthogonal to the $Q-C_{Ad}$ bond and has a π-type interaction with d_{xz}. The SALCs of the dithiolene ligands are comprised of in-plane and out-of-plane S *p* orbitals that form d_{z^2}-S_{op}, d_{xz}-$S_{ip/op}$, d_{yz}-$S_{ip/op}$, and d_{xy}-S_{ip} orbital interactions. Despite differences in apical bonding, the relative energies of the split Mo t_{2g} orbitals in desoxo complexes are comparable to those observed for mono-oxo Mo-bisdithiolene complexes. The occupied d_{xy} orbital in desoxo Mo^{IV} bisdithiolene complexes is lowest in energy and stabilized relative to the d_{xz} and d_{yz} orbitals by ∼1.5 eV. This is comparable to the $d_{xy}-d_{xz,yz}$ energy difference of ∼2 eV found for many mono-oxo Mo^{V} bisdithiolene sites, despite the lack of a strong-field apical donor ligand in the desoxo complexes.[41,42] This indicates that the desoxo Mo-bisdithiolene bonding scheme in high-symmetry geometries is not greatly perturbed by apical ligands, but instead it is the dithiolene ligands that effectively dominate the Mo ligand field. This differential dithiolene bonding is likely a balance of the dithiolene fold angles and the intra-dithiolene angles.[40,51−53]

The results of this study confirm that the apical QAd^- donor does not dominate the electronic structure of the $[Mo(QAd)(S_2C_2Me_2)_2]^{1-}$ square pyramidal site. The energies of the observed ligand-field transitions for **1**−**3** are not significantly dependent on the nature of the apical ligand, and the totally symmetric Mo−S stretching mode observed by resonance Raman spectroscopy is invariant, occurring at ∼400 cm^{-1} for all three complexes. The ∼2000 cm^{-1} energy splitting between the d_{xz} and d_{yz} orbitals, established by the energies of the $d_{xy} \rightarrow d_{xz}$ and $d_{xy} \rightarrow d_{yz}$ ligand field transitions (bands 1 and 2), is a direct result of the π interaction of the *p* orbital of the apical QAd^- donor with the d_{yz} orbital and not the d_{xz} orbital. The similar energies of these ligand-field transitions across the series of complexes provide evidence that the d_{xy} redox orbital is not directly perturbed by the nature of the QAd^- ligand in these high-symmetry complexes. Therefore, in square pyramidal geometry, the valence ionization energy and reduction potential of the Mo center is only fine-tuned by $Q \rightarrow Mo$ charge donation into the higher energy d_{z^2} and d_{xz} orbitals instead of direct destabilization of the d_{xy} redox orbital.

The complexes in this study are structurally the most accurate small molecule analogues of the reduced DMSOR active site to date. However, significant geometric rearrangements must occur from the highly symmetric square pyramidal geometries of the complexes in order to reach the putative first transition state, the binding of substrate, in an oxo transfer reaction. It is probable, considering the much slower OAT rate with respect to DMSOR enzymes, that the reorganizational energy is quite large for $[Mo(QR)(dithiolene)_2]^{1-}$ model complexes, leading to the substrate binding step being rate limiting.

Electronic Structure Influence on OAT Reactivity. Unlike the square pyramidal model complexes, crystal structures of DMSOR conserve two protein-induced distortions from this

(50) The OPT2 geometry is nearly identical to the crystal structure geometry, except that the C−O−Mo angle is much more obtuse in the crystal structure at 162°, whereas the angle optimizes to ∼135° in all of the calculations. The effect of constraining this angle in addition to the two dihedrals constrained previously was also tested and resulted in a marginal further destabilization of 0.002 eV with the HOMO essentially unchanged in character and orientation from Figure 6f.

(51) Inscore, F. E.; Knottenbelt, S. Z.; Rubie, N. D.; Joshi, H. K.; Kirk, M. L.; Enemark, J. H. *Inorg. Chem.* **2006**, *45*, 967.
(52) Joshi, H. K.; Enemark, J. H. *J. Am. Chem. Soc.* **2004**, *126*, 11784.
(53) Cooney, J. J. A.; Cranswick, M. A.; Gruhn, N. E.; Joshi, H. K.; Enemark, J. H. *Inorg. Chem.* **2004**, *43*, 8110.

Scheme 2

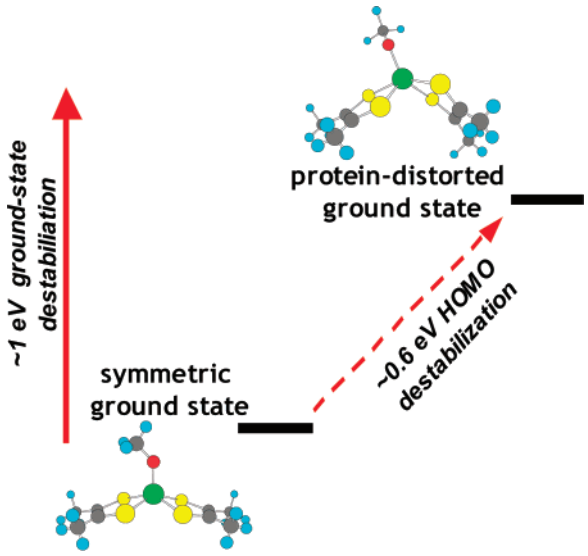

idealized geometry.[14,54] The first is a marked twist of the two dithiolene ligands relative to each other resulting from extensive hydrogen bonding of the pyranopterins to the protein. A DFT calculation of the DMSOR active site structure with a constrained dithiolene twist dihedral angle resulted in only a 0.05 eV increase in the total energy compared to the unconstrained optimized geometry. However, the other protein-induced distortion is more important and orients the conserved amino acid coordinated to Mo such that it is not perpendicular to the S_4 bisdithiolene plane but canted ~50° off the apical position (Figure 6a). A calculation constraining this coordinate led to destabilization of the ground state energy by ~1 eV, effectively decreasing the activation energy for formation of the transition state by destabilizing the ground state, as depicted in Scheme 2. Distortion-induced ligand interactions with the Mo d_{xy} orbital are clearly evident in Figure 6f, where the methoxy donor is now π-antibonding with d_{xy}. This antibonding interaction raises the energy of the HOMO by 0.56 eV, which is the donor orbital in O atom transfer reactions with substrate, thereby facilitating oxidation of the reduced active site (Figure S6). Further, this specific d_{xy}-Q_π antibonding interaction can provide substrate specificity for the enzyme and describes a plausible explicit role for different protein-derived ligands in the active sites of DMSOR enzymes.

In the DMSOR enzyme mechanism, dissociation of H_2O/OH^- from the reduced active site results in a highly distorted five-coordinate species with one lobe of the HOMO pointed toward the open coordination site, directly accessible to the attacking substrate. Indeed, protein crystal structures show that this is the most solvent- or substrate-accessible coordination site and is the binding site of the oxo ligand in oxidized DMSOR and the DMSO substrate in a DMSO-bound form.[14,55] This redox orbital orientation is not observed for high symmetry $[Mo(QR)(dithiolene)_2]^{1-}$ complexes, where the d_{xy} redox orbital is less accessible to acceptor orbitals on the incoming substrate and greater reorganization of the ligands is necessary to bind substrate.

Summary

The dithiolene ligands dominate the Mo ligand-field of desoxo Mo-bisdithiolenes in square pyramidal and distorted geometries. The redox potential of the Mo center is modulated by Q → Mo charge donation according to the nature of Q *and* its orientation relative to the d_{xy} redox orbital. The active-site distortions observed in DMSOR enzymes, relative to the square pyramidal geometries of the model complexes, act in concert to (i) allow for direct orbital interaction between the amino acid donor and the Mo d_{xy} redox orbital, (ii) provide substrate access to the redox orbital, and (iii) destabilize the ground state of the reduced active site in order to decrease the activation energy for formation of the substrate-bound transition state.

Acknowledgment. Support of this research by the National Institutes of Health (GM-057378 to M.L.K., CHE 98-76457 and CHE 00-547734 to R.H.H.) is gratefully acknowledged.

Supporting Information Available: Complete ref 32, tables of electronic absorption band maxima (T1), optimized DFT geometric parameters (T2), excitation energies and oscillator strengths from time-dependent DFT calculations (T3), figures of S_{ip} and S_{op} bisdithiolene SALCs (S1), electron density contour plots of the frontier molecular orbitals (S2−S4), DFT calculated frequencies and pictorial representation of selected vibrational modes (S5), DFT calculated molecular orbital energy diagram of OPT, OPT1, and OPT2 (S6). This material is available free of charge via the Internet at http://pubs.acs.org.

JA074691B

(54) Bray, R. C.; Adams, B.; Smith, A. T.; Bennett, B.; Bailey, S. *Biochemistry* **2000**, *39*, 11258.

(55) McAlpine, A. S.; McEwan, A. G.; Bailey, S. *J. Mol. Biol.* **1998**, *275*, 613.